Journal of Research and Applications in Mechanical Engineering
ISSN: 2229-2152 (Print); 2697-424x (Online)
(2026) Vol. 14, No. 1, Paper No. JRAME 26-14-006
[DOI: 10.14456/ jrame.2026.6]

Research Article

Numerical Analysis of Confinement Phenomenon with Reflected Shock Waves by Opposing Wall

T. Sakakura
H. Fukuoka*
A. Suda
Y. Taniguchi
K. Hiro
National Institute of Technology (KOSEN), Nara College, Nara, 639-1080, Japan

Received 6 September 2024
Revised 13 February 2025
Accepted 15 February 2025

Abstract:
We propose the shock wave confinement phenomenon as a new method for generating high-energy fields using shock waves. This study investigates the conditions for the shock wave reflection in a supersonic jets, essential for the shock wave confinement phenomenon. The parameters of this study are the pressure ratios of the high and the low-pressure chamber of the shock tube, which are 10.7, 22.6, 35.0 and 46.0, respectively. The results show that the increased pressure ratio causes the shock wave to be reflected in the jet. The non-dimensionalized thicknesses of the low acoustic impedance near the collision between the shock wave and the jet in the acoustic impedance considering the flow velocity are 1.5, 0.9, 0.6 and 0.2 when the pressure in the shock tube varies to 10.7, 22.6, 35.0 and 46.0 respectively. The thicknesses with low acoustic impedance show similar trends in the presence or absence of shock wave reflection. Therefore, the acoustic impedance, considering the flow velocity, can qualitatively explain the reflection of the shock wave to the jet.

Keywords: *Supersonic jet, Shock wave, Reflection shock wave, Confinement, Acoustic impedance*

1. Introduction

Shock waves have been the subject of extensive research up to the present day due to their potential applications. Shock waves are pressure waves caused by a sudden change in pressure, resulting in a high-energy phenomenon that raises pressure, temperature, and density after its passage. One example of its application in medicine is extracorporeal shock wave treatment for low back pain [1]. This is possible because shock waves enable non-invasive treatment. Furthermore, detonation engines, which utilize shock waves accompanied by combustion known as detonation to generate thrust, are being developed in space exploration [2]. Given the various potential applications of shock waves, there are strong demands for advancements in shock wave technology.

Among the applications of shock waves, confinement has attracted attention because of its ability to increase pressure and density. One of the studies on shock waves is the control of clusters using the confinement of shock waves generated by laser irradiation. This research has shown that local confinement of shock waves induced by laser ablation or plasma increases pressure and density within the confinement region [3][4]. Shock waves generated by plasma have also been shown to increase the pressure behind them, indicating the usefulness of spatial confinement [5]. These findings suggest that the confinement can enhance physical quantities, making it a phenomenon closely related to shock wave confinement.

A shock wave confinement phenomenon is proposed as a new application. The shock waves possess reflective properties, reflecting when they collide with objects or walls. Also, in the previous study, the experiment on the

* Corresponding author: H. Fukuoka
E-mail address: fukuoka@mech.nara.-k.ac.jp

unsteady behavior of shock waves and supersonic jets were conducted using open small-volume shock tube. As a result, it was confirmed that the shock wave was reflected multiple times between the supersonic jet and the wall surface [6]. Focusing on this characteristic, we believe that shock waves can be repeatedly reflected between the supersonic jet and the wall surface and that confinement can generate a high-temperature, high-pressure region in the desired area. Controlling this phenomenon could have potential applications in combustion technology and as a reaction field for generating new materials.

This study aims to clarify the conditions for the shock wave reflection in the jet, which is essential for understanding the shock wave confinement phenomena. However, research on the shock wave confinement phenomenon is scarce, and the conditions for its occurrence are not well understood. In another previous study, experiments showed that a change in the pressure ratio in the shock tube can change whether or not a shock wave is reflected [7]. Based on this report, numerical analysis is used to investigate pressure and density near the impact of the shock wave and jet stream, which cannot be studied experimentally. In this paper, the effect of the pressure ratio in the shock tube on the presence or absence of shock wave reflection and distributions of the physical quantity of the collision between the jet and the shock wave are discussed based on numerical analysis.

2. Calculation Conditions

2.1 Numerical Method and Boundary Conditions

In this study, numerical fluid dynamics calculations were performed to reproduce the phenomenon of a shock wave colliding with a jet stream after reflecting off a wall surface. Numerous calculations were carried out using the ANSYS Fluent 2021 code. The governing equation used was the two-dimensional axisymmetric compressible Navier-Stokes equations. The turbulence model used in this calculation is *k*-*ε*. The fourth-order Runge-Kutta method was applied for temporal discretization with an explicit scheme. The convective terms and numerical fluxes were discretized using a second-order upwind scheme and Roe's flux-difference splitting scheme. To ensure the stability of the calculations, the Courant-Friedrichs-Lewy condition was set to 0.1. Figure 1 shows the computational domain and boundary conditions. The wall conditions for the shock tube and the opposing wall in Fig. 1 were set as no-slip walls. The *x*-axis and the top of the model were subjected to asymmetry and pressure outlet conditions as other boundary conditions. The mesh generation method was generated automatically by the Ansys program. The mesh size was 0.5 mm, and a mixed mesh of triangles and quadrilaterals was used. L_h and L_b represent the high-pressure and low-pressure chamber lengths, respectively. T_h and T_b are the temperatures of the high and low-pressure chambers, set at 300 K. The computational parameters were the pressure ratio Ph/Pb within the shock tube. P_h and P_b refer to the pressures in the high-pressure and low-pressure regions within the shock tube, respectively, with P_b set to atmospheric pressure. L and D are the distance from the open end of the shock tube to the reflecting wall and the diameter of the shock tube, respectively. The diameters D, L_h and L_b were set to D = 10 mm, L_h = 10 mm, and L_b = 20 mm, respectively. This study investigated the behavior of the shock waves and jets. The pressure ratio P_h/P_b within the shock tube was varied at 10.7, 22.6, 35.0 and 46.0 for the calculations.

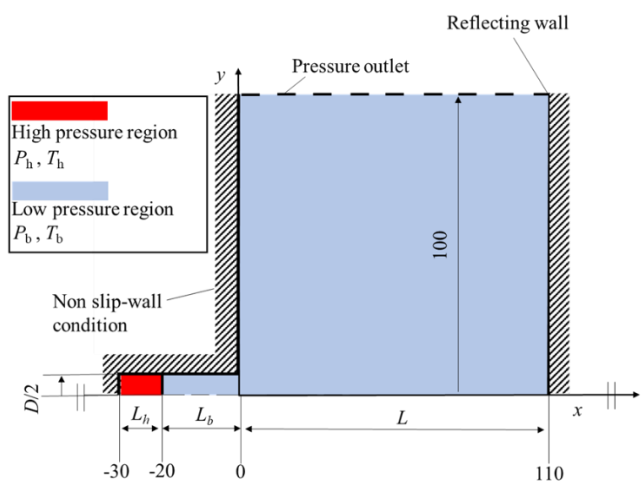

Fig. 1. Flow field and boundary conditions.

2.2 Check Validity and Mesh dependence

Figure 2 shows a model of the shock tube for verification. The calculation conditions are the same as in the present study. The mesh dependence was confirmed using a closed shock tube for comparison with theoretical values. The shock tube diameter D, high-pressure region length L_h, and low-pressure region length L_b are D = 10 mm, L_h = 20 mm, and L_b = 20 mm, respectively. The parameters of the calculations are mesh sizes of 0.5, 0.2 and 0.1 mm. Figure 3 shows the pressure distribution for the mesh size and theoretical pressure at each position at t = 15 μs. Fig. 3 shows that the pressure for mesh size 0.5 mm is approximately the same as the pressure for mesh size 0.2 mm, mesh size 0.1 mm, and the theoretical value. Therefore, the mesh size is set to 0.5 mm in this study to keep the computational cost low.

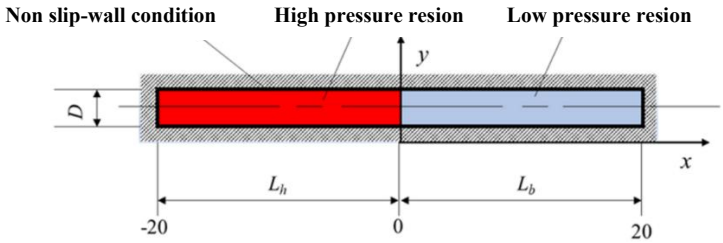

Fig. 2. Model of shock tube for verification.

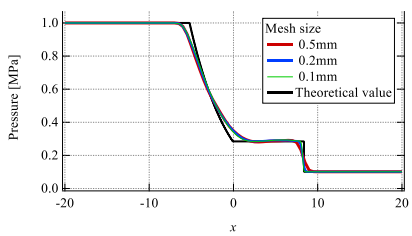

x

Fig. 3. The mesh sizes and theoretical pressures for each mesh size at each location at t = 15 μs.

3. Result and Discussion

3.1 Verification of calculation result

Figure 4 shows the flow field of the experimental and numerical. The figure is presented to examine the behavior of the jet and the shock wave in more detail. The experiment conditions, L/D and x/D are 8 and 46.0, respectively. The same conditions apply to numerical calculations. The vertical and horizontal axes are the time t and the distance value x/D, respectively. Fig. 4 shows that the shock wave and the jet reach the reflective wall at t = 120 μs and t = 275 μs for both experimental and numerical analysis. Thus, the numerical analysis confirms the qualitative agreement with the experiment under these conditions.

3.2 Typical Flow Field

Figure 5 shows the temporal evolution of the flow field using computational Schlieren imaging at a pressure ratio of P_h/P_b = 46.0. The time t = 0 μs represents the time of the diaphragm ruptures in the shock tube. The arrows in the figure indicate the head of the shock wave. As shown in Fig. 5(a), at x/D = 5.1 and x/D = 7.5 along the central axis at y/D = 0, the head of the jet and the shock wave induced by the jet can be observed. These correspond to the jet ejected

from the shock tube and the shock wave induced by the jet stream. In Fig. 5(b), the head of the reflected shock wave can be observed at $x/D = 6.8$ along the central axis at $y/D = 0$. This indicates that the shock wave from the open end of the shock tube toward the reflective wall is reflected off the wall and propagates back toward the open end. In Fig. 5(c), the shock wave reflected from the wall collides with the jet at $x/D = 6.0$. In Fig. 5(d), the shock wave reflected by the jet can be observed at $x/D = 7.0$ along the central axis at $y/D = 0$.

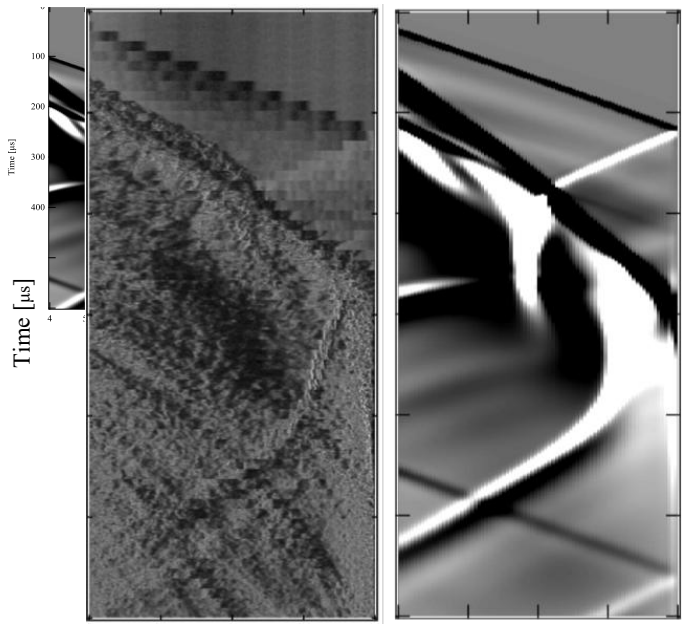

Fig. 4. Time history of Schlieren and Computer schlieren for $L/D = 8$ and $P_h/P_b = 46.0$.

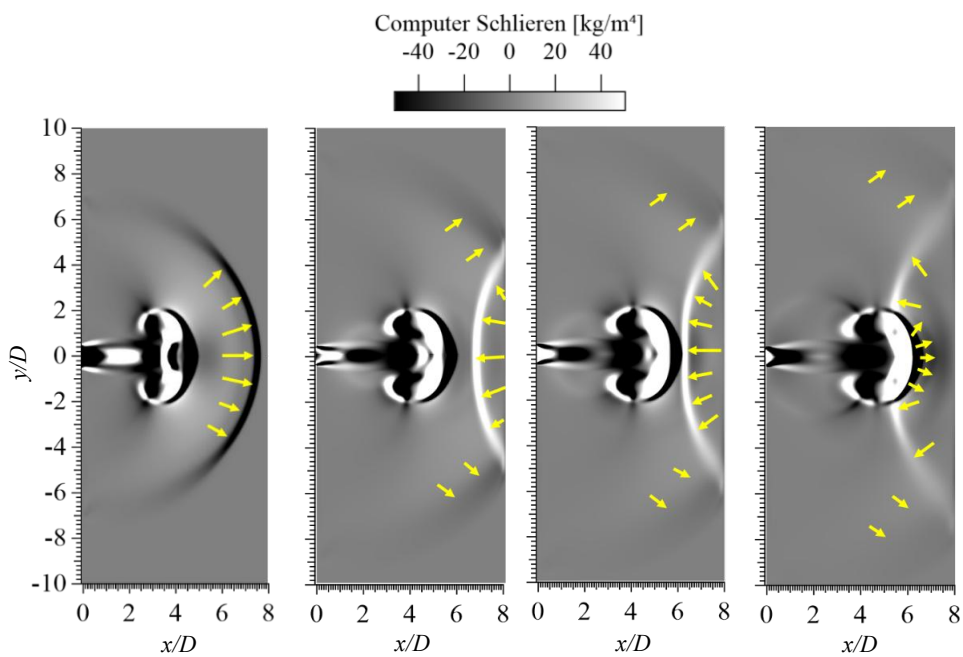

Fig. 5. Computer schlieren for $L/D = 8$, $P_h/P_b = 46.0$

The *x-t* diagram is presented to examine the behavior of the jet and the shock wave in more detail. Figure 6 was created for P_h/P_b = 46.0 by sequentially extracting computed Schlieren images along the central axis and arranging them in a continuous sequence up to t = 500 μs. Fig. 6 shows that at t = 200 μs, 254 μs and 300 μs, the shock wave reaches the reflective wall, collides with the jet, and reaches the wall, respectively. Additionally, the jet reaches the reflective wall at t = 275 μs. Therefore, numerical calculations confirm that the shock wave is reflected multiple times between the reflective wall and the jet stream.

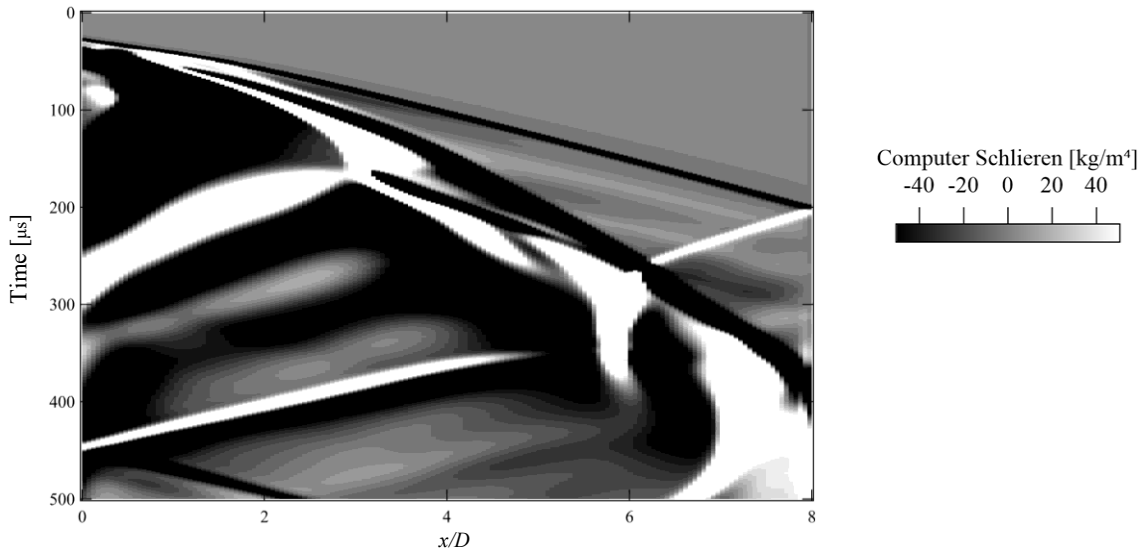

Fig. 6. Time history of Computer schlieren for L/D = 8 and P_h/P_b = 46.0.

3.3 Influence of Pressure Ratio on the Shock Wave Reflection at the Jet

We investigate the effect of the pressure ratio P_h/P_b within the shock tube on the reflection of shock waves in the jet. Figure 7 shows the *x-t* diagrams of computational Schlieren images for P_h/P_b = 10.7, 22.6 and 35.0. As shown in Fig. 7, in the cases of P_h/P_b = 10.7, 22.6 and 35.0, like P_h/P_b = 46.0, the shock wave reaches the reflective wall, reflects at the wall, and subsequently collides with the jet can be observed. For P_h/P_b = 35.0, the moment at t = 325 μs when the shock wave reflected within the jet reaches the reflective wall can also be observed. On the other hand, for P_h/P_b = 10.7 and 22.6, it is not confirmed that the shock wave reflects in the jet. From this, it can be confirmed that the shock wave reflects due to the jet at higher pressure ratios.

3.4 Acoustic Impedance with Consideration of Flow Velocity at Each Pressure Ratio

Based on the above, it was found that the presence or absence of shock wave reflection in the jet changes with an increase in the pressure ratio. Generally, the presence or absence of the shock wave reflection is well explained by an acoustic impedance. Acoustic impedance is a measure of the ease of wave propagation. The evaluation of reflection by acoustic impedance is determined by the difference in acoustic impedance of each medium when a shock wave is incident between two media without flow velocity. Since this report is concerned with shock waves incident on a jet, the evaluation is performed for each region inside and outside the jet. In this study, the flow field is induced by shock waves and jets, so the acoustic impedance I' is used, as shown in Equation (1), which is the speed of sound minus the flow velocity. In the equation, ρ, a and v represent the density, the sound speed, and the flow velocity, respectively.

$$I' = \rho|a - v| \tag{1}$$

Figure 8 shows the flow fields based on acoustic impedance. The flow fields represent the state just before the collision between the jet and the shock wave. In the case of Fig. 8(d), the high acoustic impedance region can be observed at y/D = 0, x/D = 4.2–4.5. This indicates the high acoustic impedance region in the center of the jet. Furthermore, the three-layer structure of high, low, and high acoustic impedance regions is not formed from the center of the jet. In the cases of Fig. 8(b) and (c), a similar three-layer structure is not observed as in Fig. 8(d). On the other

hand, in Fig. 8(a), the high acoustic impedance region is observed at the center of the jet. Additionally, in Fig. 8(b), (c) and (d), the width of the low acoustic impedance region surrounding the center of the jet is 0.9, 0.6 and 0.2 at $y/D = 0$, respectively. From this phenomenon, it was found that the width of the low acoustic impedance layer becomes thinner as the pressure ratio increases. Therefore, it is suggested that the reflection of the shock wave in the jet is caused by the three-layered structure of acoustic impedance, and the low acoustic impedance layer is thin.

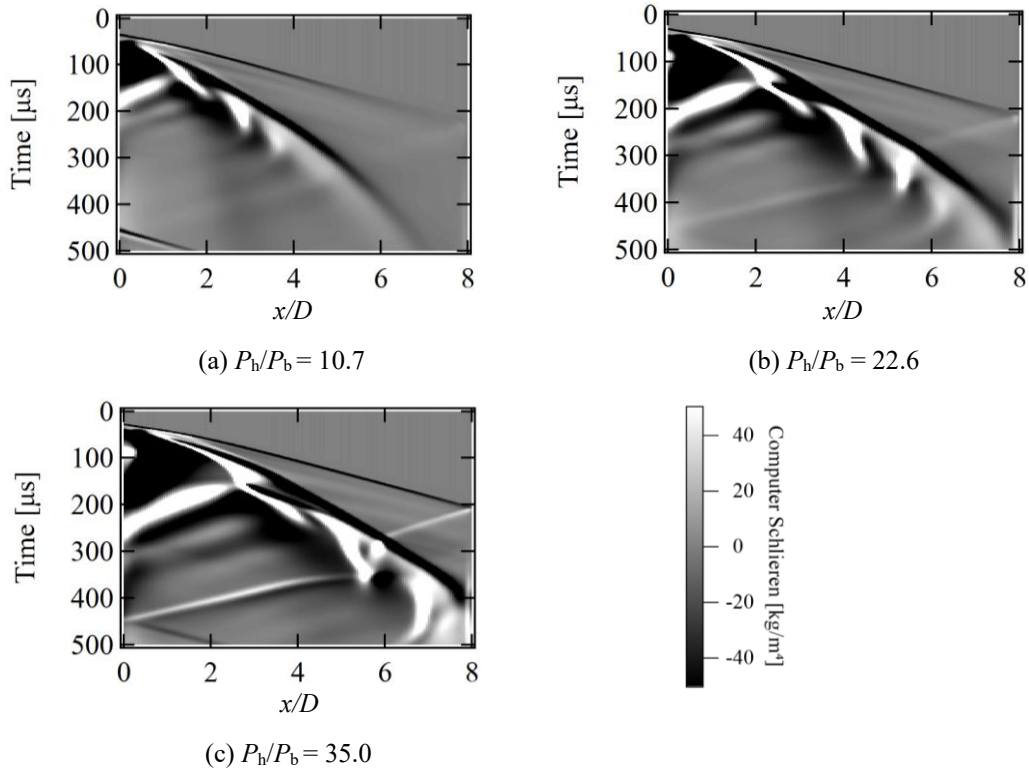

(a) $P_h/P_b = 10.7$ (b) $P_h/P_b = 22.6$

(c) $P_h/P_b = 35.0$

Fig. 7. Time history of Computer schlieren for $L/D = 8$.

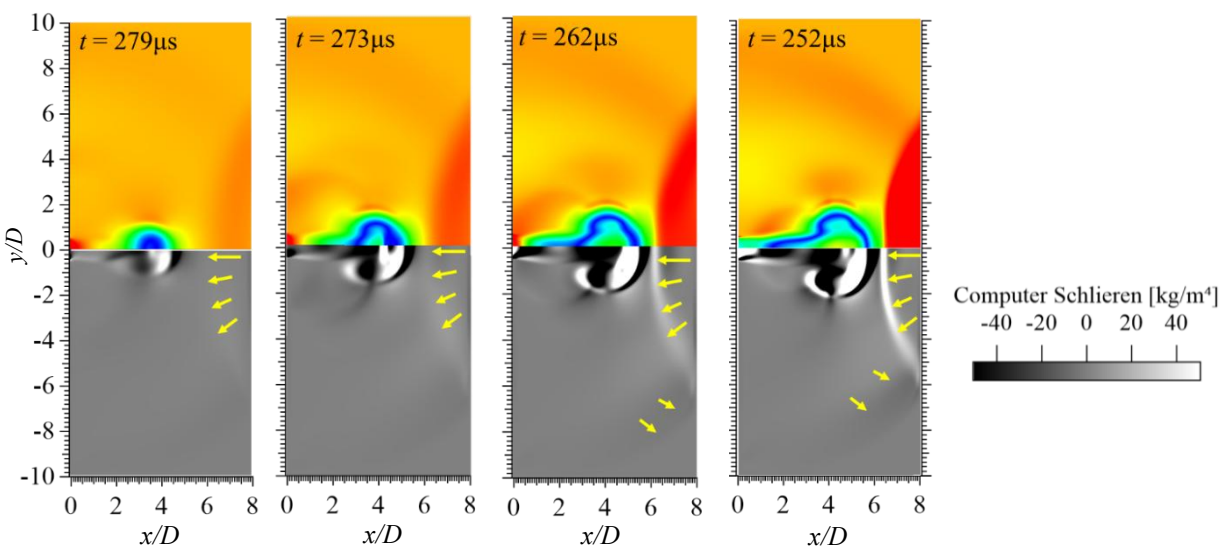

(a) $P_h/P_b = 10.7$ (b) $P_h/P_b = 22.6$ (c) $P_h/P_b = 35.0$ (d) $P_h/P_b = 46.0$

Fig. 8. Acoustic Impedance and Computer Schlieren for $L/D = 8$, $P_h/P_b = 46.0$.

4. Conclusion

This study aims to clarify the reflection conditions of shock waves in a jet flow. A numerical analysis was conducted on a flow field with a shock tube and a reflective wall to achieve this. The governing equations are the two-dimensional axisymmetric compressible Navier-Stokes equations. The parameter of interest is the pressure ratio within the shock tube, P_h/P_b, ranging from 10.7 to 46.0. As a result, it was found that for P_h/P_b = 35.0 and 46.0, the shock waves reflected from the reflective wall were again reflected by the jet. On the other hand, for P_h/P_b = 10.7 and 22.6, it was confirmed that the shock waves were not reflected in the jet. This is due to the presence or absence of reflection changes with an increased pressure ratio. Additionally, for P_h/P_b = 22.6, 35.0 and 46.0, it was observed that the three-layer structure of high, low, and high acoustic impedance is formed from the center of the jet. Furthermore, it was found that the thickness of the low acoustic impedance layer decreases as the pressure ratio increases. These observations consider that the reflection of the shock wave in the jet is influenced by the three-layer structure of acoustic impedance and the thickness of the low acoustic impedance layer.

Nomenclature

L_h	high-pressure chamber lengths, m
L_b	low-pressure chamber lengths, m
T_h	the temperatures of the high-pressure chambers, K
T_b	the temperatures of the low-pressure chambers, K
P_h	high-pressure regions within the shock tube, Pa
P_b	low-pressure regions within the shock tube, Pa
L	distance from the open end of the shock tube to the reflecting wall, m
D	diameter of the shock tube, m
P_h/P_b	pressure ratio within the shock tube

References

[1] Jinhui M, Yan Y, Bailiang W, Wei S, Debo Y, Weiguo W. Effectiveness and safety of extracorporeal shock wave treatment for low back pain: a systematic review and meta-analysis of RCTs. International Journal of Osteopathic Medicine. 2022;43:39–48.

[2] Zezhong Y, Bo Z. Numerical and experimental analysis of detonation induced by shock wave focusing. Combustion and Flame. 2023;251:1–12.

[3] Chong L, Jianmei W, Xinwei W. Shock wave confinement-induced plume temperature increase in laser-induced breakdown spectroscopy. Physics Letters A. 2014;378:3319–3325.

[4] Junfeng S, Jin G, Qiuyun W, Anmin C, Mingxing J. Spatial confinement effect on CN emission from nanosecond laser-induced PMMA plasma in air. Optics and Laser Technology. 2022;207:1–7.

[5] Thomas D, Brian M, Derek AT, Murthy MD, Peri I, Ivin V, Cetin C. Pressure amplification of laser-induced plasma shockwaves with shock tubes for nanoparticle removal. Journal of Adhesion Science and Technology. 2007;21:67–80.

[6] Miyaoku K, Fukuoka H, Nakamura S, Enoki S, Hiro K, Yao A. Study on shock wave confinement using small high-pressure chamber shock tube. Proceedings of the 31st International Symposium on Transport Phenomena. 2020:131.

[7] Deyama K, Fukuoka H, Suda A, Nakamura S. Experimental observation of collision process between converging shock wave and supersonic jet. Proceedings of the 9th Asian Joint Workshop on Thermophysics and Fluid Science. 2022:1–3.